Marine Pollution Bulletin 115 (2017) 105–114

Contents lists available at ScienceDirect

Marine Pollution Bulletin

journal homepage: www.elsevier.com/locate/marpolbul

The use of wide-band transmittance imaging to size and classify suspended particulate matter in seawater

E.J. Davies*, P.J. Brandvik, F. Leirvik, R. Nepstad

Department of Environmental Technology, SINTEF Materials and Chemistry, Brattorkia 17c, Trondheim, Norway

ARTICLE INFO

Article history:
Received 14 October 2016
Received in revised form 20 November 2016
Accepted 27 November 2016
Available online 5 December 2016

Keywords:
Monitoring
Measurement
Oil
Gas
Size distribution
Mine tailings

ABSTRACT

An *in situ* particle imaging system for measurement of high concentrations of suspended particles ranging from 30 μm to several mm in diameter, is presented. The system obtains quasi-silhouettes of particles suspended within an open-path sample volume of up to 5 cm in length. Benchmarking against spherical standards and the LISST-100 show good agreement, providing confidence in measurements from the system when extending beyond the size, concentration and particle classification capabilities of the LISST-100. Particle-specific transmittance is used to classify particle type, independent of size and shape. This is applied to mixtures of oil droplets, gas bubbles and oil-coated gas bubbles, to provide independent measures of oil and gas size distributions, concentrations, and oil-gas ratios during simulated subsea releases. The system is also applied to *in situ* measurements of high concentrations of large mineral flocs surrounding a submarine mine tailings placement within a Norwegian Fjord.

1. Introduction

Many types of marine pollution exists in the form of *particles* suspended within the water column. Examples include: oil droplets and gas bubbles (Johansen et al., 2013; Zhao et al., 2014), mineral mining waste (Ramirez-Llodra et al., 2015), organo-metallic colloids (Turner and Millward, 2002), microplastics (Pham et al., 2014; Wright et al., 2013), and polluted sediments (Superville et al., 2015). In order to understand the transport and fate of such pollutants, it is of critical importance to understand their particle nature. Such studies are impeded by the fragile nature of suspended particles, which means that direct sampling will often lead to changes in the size and shape. Thus, there is a need for *in situ* measurement techniques. The challenge in obtaining direct measurements is to cover the large range of particle sizes, concentrations and types present in polluted seawater (Johansen et al., 2013).

The size range of particulate pollutants spans many orders of magnitude, from nano-sized pollutants (the scale of bacteria) up to multiple-millimetre oil droplets (the scale of zooplankton). This range cannot be covered by one instrument alone and therefore *in situ* monitoring must constitute a suite of instruments, each using different techniques to capture information within a relative narrow size range. Laser diffraction is adopted by the commonly-used LISST-100 (Agrawal and Pottsmith, 2000), and provides a good mechanism for undisrupted *in situ* measurements, but the size range for these measurements is restricted to particles between 2.5–500 μm in diameter (Davies et al., 2012).

In addition to the complexities of covering a large range of sizes, high concentration also poses a challenge in cases of acute point-source discharges, where the concentrations near the source are much higher than the typical oceanic or coastal concentrations of suspended particles (Graham et al., 2012) for which standard instruments, such as the LISST-100, are designed. In some cases, such as a subsea oil blowout, challenges associated with large volume concentrations can be overcome by effectively increasing the height of measurement above the release plume to enable sufficient dilution. This approach is adapted in small-scale experimental releases such as those reported by Brandvik et al. (2013). However, this approach necessitates a significant experimental down-scaling at the point of release so that both the droplet sizes and concentrations fall within the measurable range of the LISST-100. In the case of studies of subsea releases, this has uncovered a need to extend droplet measurements to larger sizes and higher concentrations so that experimental conditions can be more closely coupled to realistic scales.

Imaging, whether by way of holography or standard lens-based systems, is currently the only solution to these challenges, as acoustic methods are limited to coarse, or bulk, statistics of the measured

* Corresponding author.
E-mail address: emlyn.davies@sintef.no (E. Davies).

http://dx.doi.org/10.1016/j.marpolbul.2016.11.063

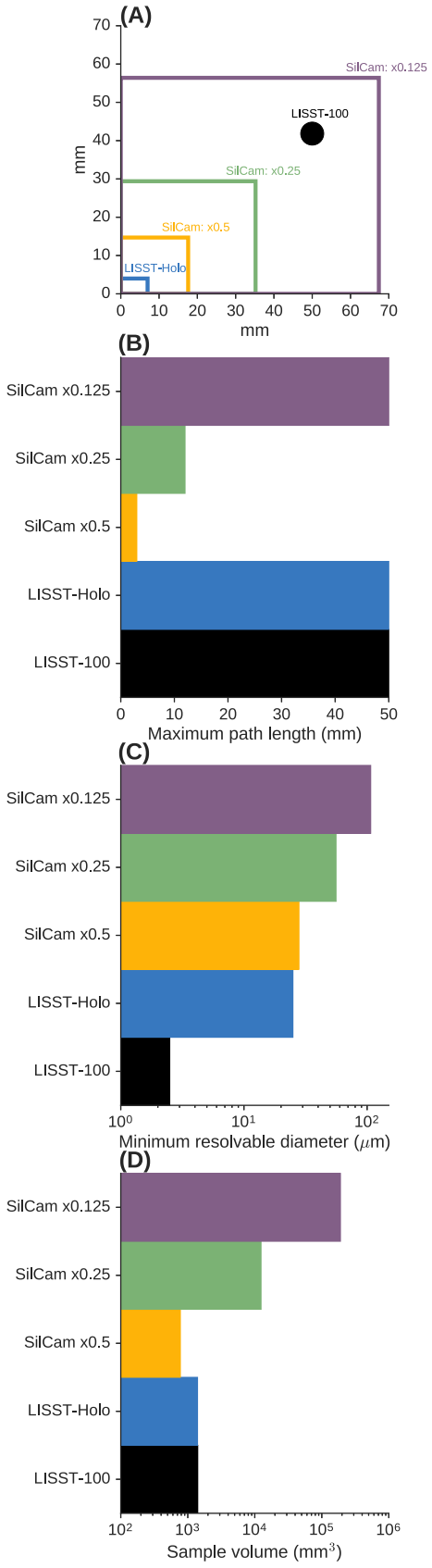

Fig. 1. System parameters of the three magnification options possible with the SilCam, compared to the standard configuration of the LISST-Holo and LISST-100. A: Sample volume cross-sectional area. B: Maximum path length. C: Minimum resolvable spherical particle. D: Total sampling volume.

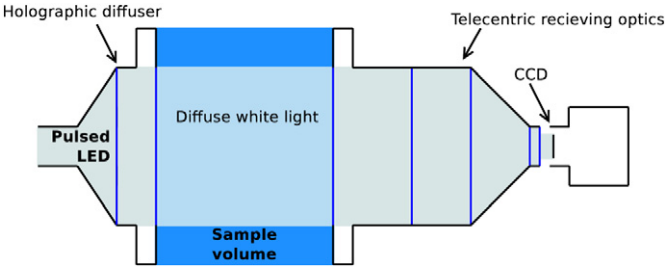

Fig. 2. Schematic illustration of the optical configuration of the silhouette system.

particle populations (Thorne and Buckingham, 2004; Thorne and Hanes, 2002). Conventional lens-based imaging of suspended particles often suffers from limitations related to depth-of-field, particle occlusion, and perspective errors. These errors can be overcome by the use of holographic imaging, which effectively enables refocussing of every identified particle during post-processing. Digital holographic imaging, adopted by the commercially-available LISST-Holo (Graham and Nimmo-Smith, 2010), has offered a viable method to extend the 500 μm limit of the LISST-100 and provide measurements of particles of up to just over 4 mm. While the LISST-Holo provides a substantial step forward in our ability to monitor marine suspended particles, the usable upper size limit for automatically processed size distributions is closer to 2 mm due to over-segmentation of large particles during reconstruction and binerization (Davies et al., 2015). Under-sampling is also a challenge for measurements of large particles, as only one or two particles of mm-scale can fall within the sample volume (4 × 6× 50 mm) at any one time. In addition, a path reduction module (which reduces the sample volume to 4 × 6× 25 mm) is required to reduce the likelihood of overlapping particles, but its use further exacerbates the problem of under-sampling.

When concentrations are high and droplet sizes are large (mm-scale), the advantages of the long path length and small pixel size of the LISST-Holo are reduced. To address this problem we have developed a new imaging system designed to quantify high concentrations of suspended particulates within the range of ~30–12,000 μm, as a complimentary tool to existing commercially-available instruments such as the LISST-100 and LISST-Holo (Sequoia Scientific Inc.). This new *in situ* particle imaging system is specifically designed to combat challenges associated with standard imaging or video cameras (e.g. Curran et al., 2003; Mikkelsen et al., 2005, 2004; Milligan, 1996) through the use of carefully configured backlighting and telecentric receiving optics. The result is an optical hardware configuration that ensures low-noise images where all particles in the sample volume are sharp, in-focus and free from the errors with perspective that are associated with standard lenses. In addition to the extension of the upper limit to measurable particle sizes, the system is also able to characterise particle types based on optical properties, such that particles of equivalent geometry can be separated. This has been used to quantify independent size distributions and concentrations of oil droplets and gas bubbles within mixed releases, enabling the two populations to be analysed independently and providing measurements of oil-gas ratio.

This article outlines the materials used in design and construction of the imaging system, the procedures adopted in processing the data

Fig. 3. Photograph of the system within a high-pressure housing.

it obtains, and an evaluation of the performance of the instrument for a variety applications relevant for marine pollution.

2. Materials and procedures

The imaging system (called the 'SilCam' for the sake of brevity) operates using the principle of backlighting to create quasi-silhouettes of particles suspended between the light and the camera. 15 images are taken per second, with a path length that is adjusted according to the concentration and also to ensure that the largest particles are able to pass through the sample volume with minimal disruption. Three different magnifications (×0.5, ×0.25, and ×0.125) can be used (Fig. 1), each with resulting in pixel sizes of: 7.2 μm, 14.4 μm, 27.5μm, yielding field of views of: 17.6 × 14.7 mm, 35.2 × 29.4 mm, and 67.4 × 56.4 mm respectively, and minimum quantifiable diameters (D_{min}) of: 28 μm, 56 μm, 107 μm, as per Eq. (1).

$$D_{min} = 2\sqrt{\frac{12P^2}{\pi}} \quad (1)$$

where P is the pixel size.

Errors due to out-of-focus particles are removed by use of telecentric receiving optics that have a depth-of-field that is equal to- or wider than the physical restriction to the instrument path length (i.e. the gap between the illumination and camera housing windows). The path lengths chosen therefore vary from approximately 3 mm for the highest magnification and highest concentration to 50 mm for the lowest magnification and lowest concentration environments.

Particle dimensions are quantified and used to determine size distributions and concentrations. Equivalent circular diameters for every particle are counted, by volume concentration, into log-spaced size bins that match the LISST-100 (Type-C spherical inversion) and extend a further 21 size classes larger than the 500 μm upper limit of the LISST-100, yielding a total of 53 log-spaced size classes - albeit with the smallest out-of-range classes being left empty such that comparison with the LISST-100 and LISST-HOLO instruments is possible.

To study combined releases of oil and gas, a particle identification scheme was developed to distinguish between oil droplets and gas bubbles. This makes use of an identification method based on signatures of transmitted light of different wavelengths through each individual particle recorded. As these transmitted signatures are unique to a specific particle absorption characteristic (i.e. optical properties related to composition), it is possible to automatically separate oil droplets, gas bubbles and oil-coated gas bubbles of equal size and shape. This identification enables calculations of distinct distributions for oil droplets and gas bubbles (including oil-coated gas bubbles) from a mixed release.

2.1. System configuration

The hardware configuration of the SilCam is targeted at combating the challenges associated with conventional imaging systems, through the use of telecentric receiving optics. This removes parallax effects and subsequent position-dependent magnification errors, associated with standard lenses. The result is an image in an orthogonal projection, so particles close to the camera-end of the sample volume appear the same size as particles further away. In addition, telecentric lenses have a relatively large depth-of-field, enabling the system, with an appropriately restricted path-length, to ensure that all particles in the sample volume are in focus. In effect, this use of telecentricity achieves, via hardware, what holography achieves in post-processing, only without the ability to determine z-axis particle positions but with the benefit of very clean images without the speckle noise associated with digital in-line holography.

In addition to the choice of receiving optics, it is critical to obtain images with a homogeneous, diffuse and clean background illumination. This simplifies data treatment and subsequently increases the accuracy and reliability of particle measurements. Background illumination consists of a large, high-power white LED array, the beam of which is expanded and diffused, using a holographic diffuser, immediately prior to the housing window in order to reduce radial variance surrounding the centre of the LED cluster (Fig. 2). The incident light then passes through the sample volume, through the near-side

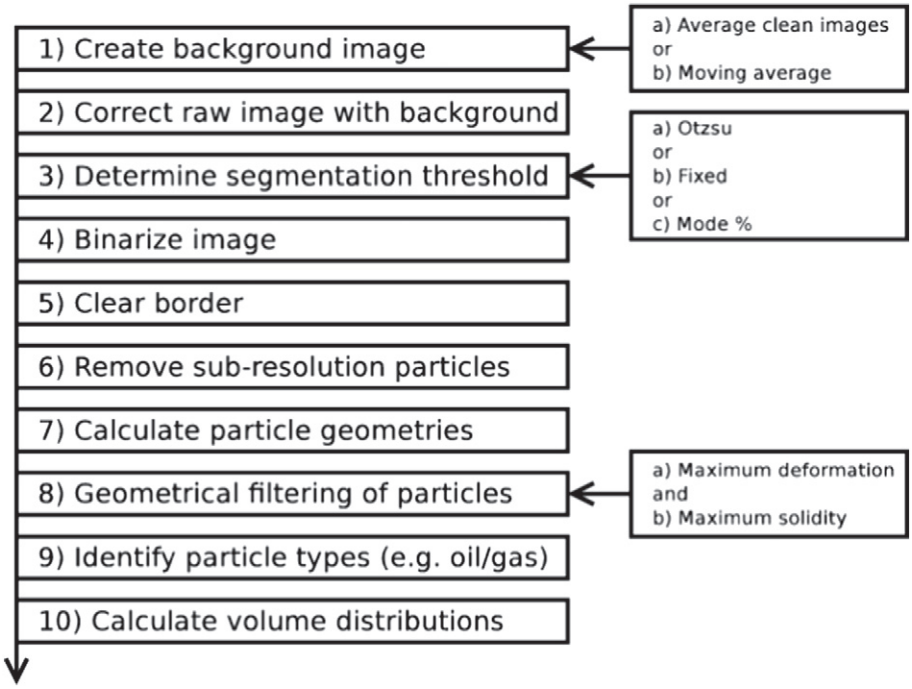

Fig. 4. Process flow diagram for analysis of images.

housing window and into the telecentric receiving optics, which is attached to a colour CCD (Charge-Coupled Device) camera. The combination of telecentric receiving optics with multi-wavelength (i.e. colour) imaging sensor and wide-band diffuse back-lighting enables the retrieval of an optical signal that is related to the spectral transmittance through the water a particles at each pixel position. Images are recorded onto solid-state disk to enable continuous operation at 15 Hz without the need for buffering. The optical configuration is mounted into two underwater housings (one for the illumination and one for the receiving optics and camera), which are rated to 3000 m depth (Fig. 3).

2.2. Data treatment and analysis

Treatment of the data is relatively simple, with the basic workflow outlined in Fig. 4. The following main processing steps are applied to each image recorded by the silhouette system: 1) Each image is corrected by a clean background to reduce noise; 2) The corrected image is segmented (binarized) to produce a logical image (zeros and ones) of the particles detected; 3) Particles in the binary image are then counted and particle properties (geometry and particle type) are calculated for each particle; 4) The particle size distribution is calculated by counting Equivalent Circular Diameters (ECD) into their appropriate volume size class (log-spaced size bins as per the LISST-100 and LISST-HOLO, but extending up to 12,000 μm).

The background image used for correction of each raw image can either be calculated from an average of images recorded in clean water or from a moving-average of images either side of each raw image. The correction of images using a 'clean' background removes noise and gradients in background illumination. The advantage of using a moving-average is that particles or oil droplets that adhere to the housing windows are removed from the analysis. This is particularly important for high-concentration measurements of oil where fouling is often problematic. In fact, fouling by oil in high concentration releases of large oil droplets is so problematic, that an *in situ* water-jet cleaning system is often used to wash the windows periodically during an experiment.

Fig. 5 shows the background image, I_0 (A), the raw image, I (B), and the corrected image, C (C). The initial segmented image (prior to geometrical filtering) is shown in Fig. 5D.

The corrected image ($C(i,j,\lambda)$) can be calculated as follows (Eq. (2)):

$$C(i,j,\lambda) = \frac{I(i,j,\lambda) - I_D(i,j,\lambda)}{I_0(i,j,\lambda) - I_D(i,j,\lambda)} \quad (2)$$

where I is the raw intensity in position i, j as a function of wavelength (λ). I_0 is the reference illumination intensity in position i, j as a function of wavelength (λ). I_D is a dark image.

In reality, λ is a broad band of wavelengths, dependent on the camera sensor used. Variation in sensitivity over different wavelengths is corrected for during the background correction (Eq. (2)). In the future, the use of a simple RGB colour CCD could be replaced by a multi- or hyper-spectral sensor, which in combination with appropriate illumination could significantly enhance the spectral transmittance information that can be retrieved from the system.

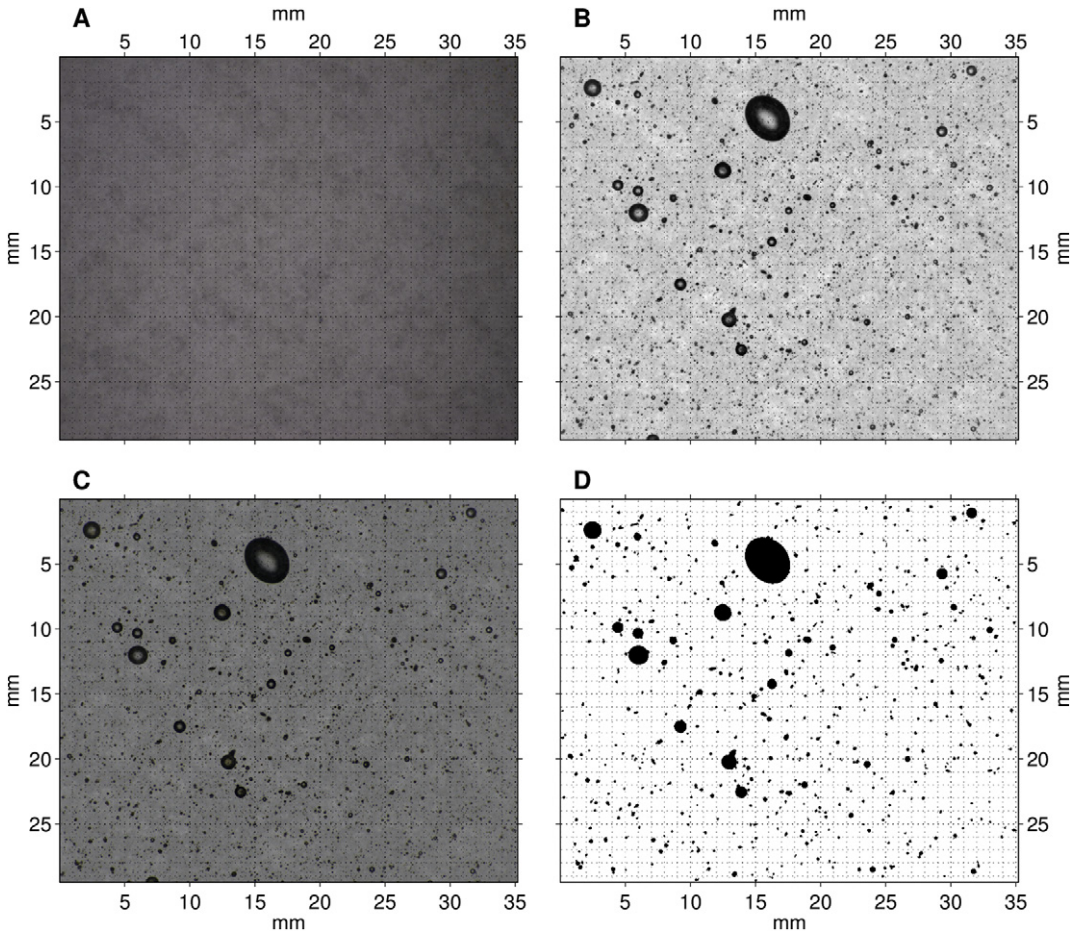

Fig. 5. A: Background image (I_0); B: Raw image (I); C: Corrected image (C); D: Initial segmented image.

2.3. Classification of oil and gas

Automated classification of suspended marine suspended particle measured *in situ* has been possible using geometrical properties of identified particles. However, this becomes a challenge for differentiating between oil droplets and gas bubbles as both particle types are close to spheroidal in shape. The use of the unique indicators in the transmitted colour through the images particles ($C(i,j,\lambda)$), obtained with the system, now presents a solution to separating particle types with similar geometries but varying optical properties. The use of the total intensity over all wavelengths did not provide reliable results in situations where gas bubbles were coated with a thin layer of oil. A simple approach is used for separating oil droplets and gas bubbles, based on the radial intensity of the green light through each particle,

$$I'(x) = \sum_{J=1}^{n_y} C(x, y_{(J)}, \lambda_{(Gr)}), \tag{3}$$

where $I'(x)$ is the summed intensity of the green channel through all y pixels of the corrected and masked particle image (C). A filtered version of $I'(x)$ is plotted in Fig. 6C and D. The peaks and troughs in this filtered signal of $I'(x)$ are identified and their number, separation and amplitude are used to determine the presence, or not, of gas. Fig. 6C and D show this function of the transmitted intensity of green light for oil (C) and oil-coated gas (D), the associated images of which are shown in A and B, respectively. A prominent peak in intensity is present in the intensity profile of the gas, and remains as a single trough in the case of oil. These differences between the intensity signal of the oil and gas remain consistent over all sizes above the minimum resolvable diameter of the system (Eq. (1)). In the case of separating oil, gas and oil-coated gas, the use of a single, green waveband was sufficient. However, there remains potential for more advances classification schemes to utilise an equivalent signal from multiple wavebands if discriminating between more subtle differences in particle properties is necessary. It is also worth noting that Eq. (3) only produces a reliable signal if the particles in question contain a degree of transparency. All particles that are totally opaque, or 100% absorbing over all measured wavelengths, would have to be classified together if their geometries were equivalent.

Fig. 7 shows a segmented image of identified oil (black) and gas (blue) particles, which are subsequently used for calculating the population-independent geometrical statistics and volume distributions.

3. Results & discussion

3.1. Benchmarking

Measurements of spherical standards were used to confirm accurate size measurements from known, mono-disperse distributions of suspended particles in water. Standards were injected above the sample volume and left to settle through the imaging area. The processing routines outlined earlier were used to calculate the size distributions. Resulting measured size distributions for 80 μm and

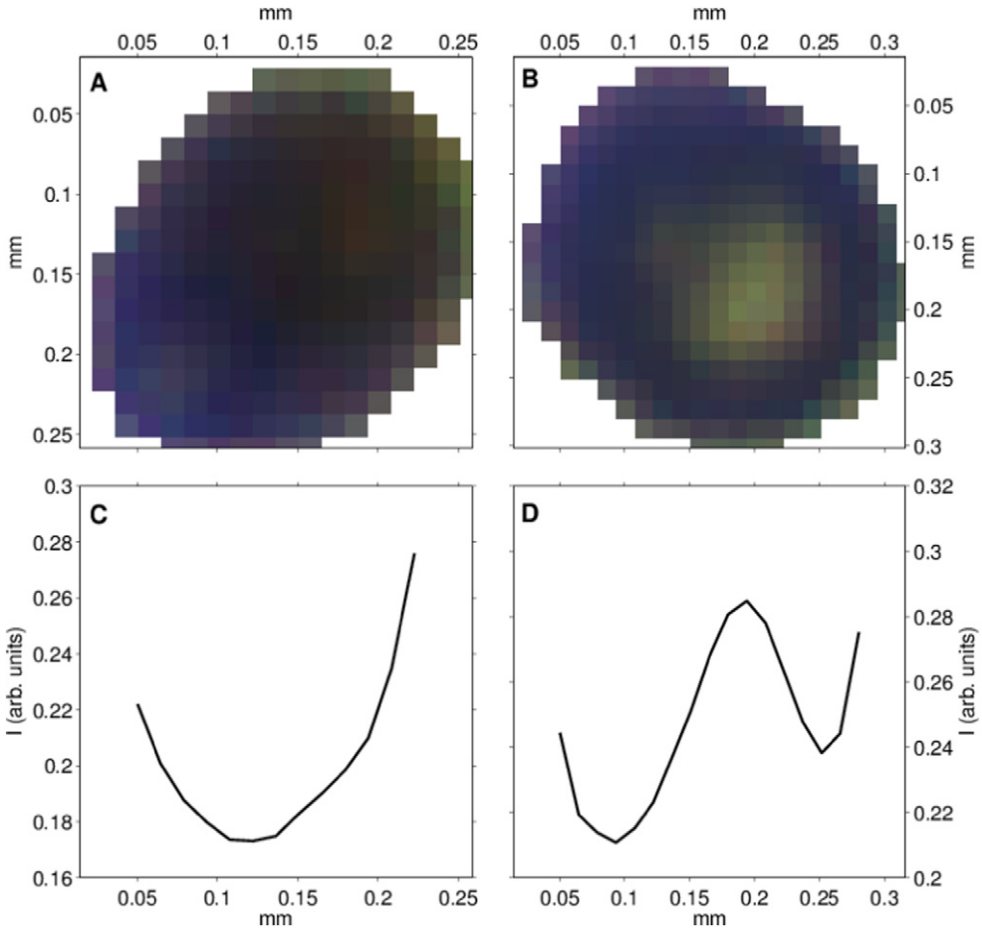

Fig. 6. Example of the intensity summation of the transmitted green light through an oil droplet (left) and an oil-coated gas bubble (right).

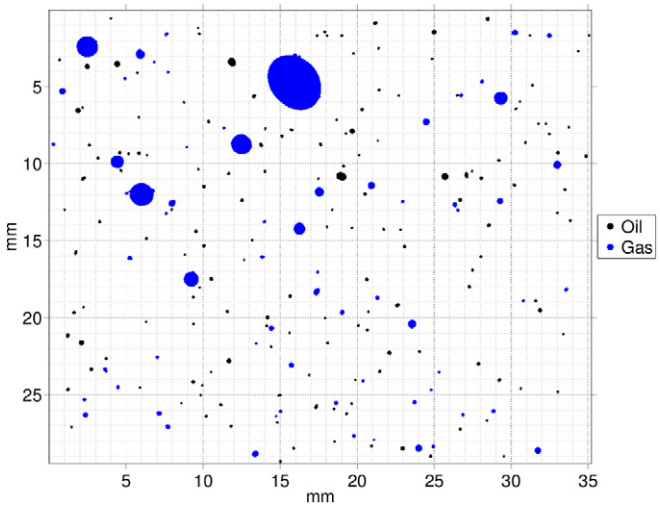

Fig. 7. Example composite segmented image showing identified gas bubbles in blue and oil droplets in black.

360 μm standards are shown in Fig. 8. Good agreement in the median sizes for the two standards is clearly evident. Some deviation in the exact position of the peaks of the measured distributions, in comparison to the expected mode of the standards, is likely due to statistical artefacts in binning the counted diameters into the log-spaced size classes.

Simultaneous measurements of oil droplets recorded by a LISST-100 and the SilCam from an experimental release of oil are shown in Fig. 9. The size ranges of the two instruments are indicated above the plot. Both instruments recorded very similar size distributions, with the peak in volume concentration (or modal size) occurring in same size-class for both instruments. A tendency for slightly higher relative concentrations of the smaller particles to be reported by the LISST-100 is apparent, although the differences here are small in comparison to the temporal variability within the highly dynamic plume in which the instruments were placed.

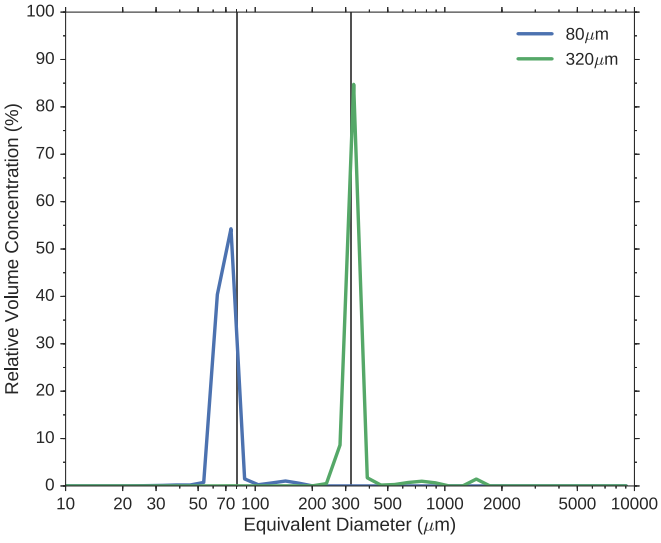

Fig. 8. Measured size distributions from two mono-disperse spherical standards of 80μm (blue) and 360μm (green).

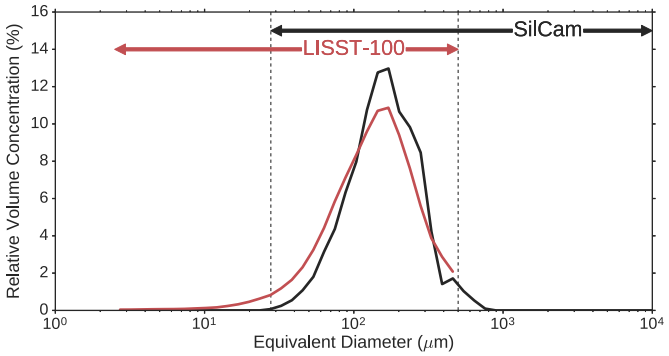

Fig. 9. Oil droplet size distributions from the LISST-100 and SilCam while deployed alongside each other within an experimentally-created rising plume of released oil. The distributions presented are recorded over an identical 30-second period. Black dashed lines indicate the limits of the size classes that are common to all three instruments.

3.2. Measurements of mixed oil and gas

Separate size distributions of oil droplets and gas bubbles are obtained from classified images (as demonstrated in Fig. 7). Example size distributions of oil and gas from a mixed experimental release are shown in Fig. 10. The figure shows that the two independent distributions have similar median diameters, and as such the total concentration of all particles is not necessarily bi-modal during mixed releases of oil and gas. This can be seen by the grey line which indicates the total distribution of both oil and gas. Therefore, it is important that the oil and gas are separated using a method that is not size-dependent, i.e. it is not possible to separate oil and gas by searching for modes in the total, combined size distribution.

By integrating the volume distributions of the independently-classified oil and gas particles, it is possible to extract their respective concentrations. The ratio of the two concentrations, thus, provides a measure of the oil-gas ratio. The relationship between the experimental set-point for the oil-gas ratio and the measured oil-gas ratio, for a series of experiments that cover a range of gas types and dispersant injection, is shown in Fig. 11.

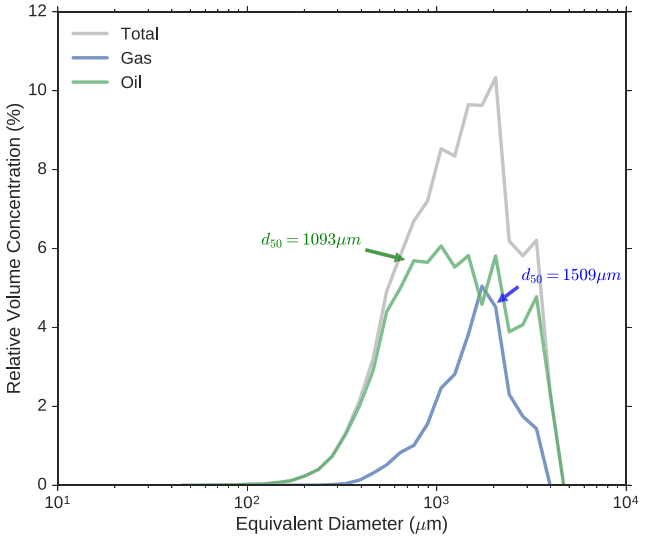

Fig. 10. Example classified size distributions of mixed oil and LNG, averaged over a 30-second period. The concentrations of oil and gas are normalised by the total concentration of all particles to produce the relative percentage distribution. The total size distribution of both oil and gas is shown by the grey line. The measured oil-gas ratio is 2.7.

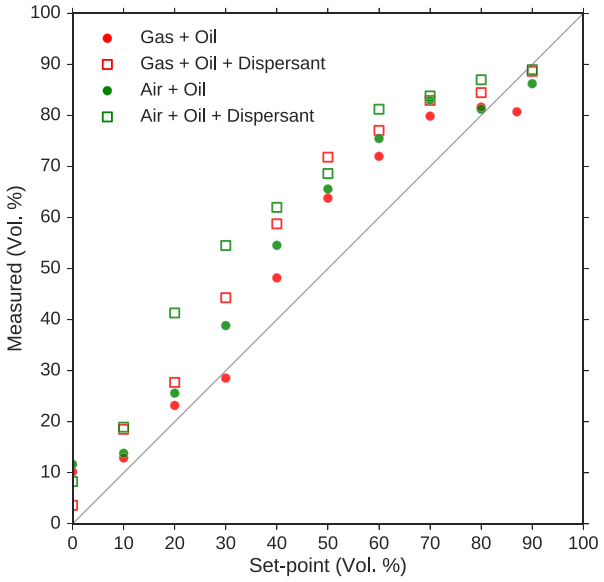

Fig. 11. Comparison of the experimental set-point for the oil-gas ratio and the oil-gas ratio measured using the SilCam.

Due to lack of a reliable alternative method for independently quantifying the size distribution and concentration of oil and gas within a simulated blowout, it is challenging to conduct a validation of the results. As such, comparison between the experimental set-point for the released oil-gas ratio and the measured equivalent is deemed useful in verifying that the processed SilCam data follow the expected trends. Many uncertainties are therefore difficult to quantify in such a comparison. For example, the set-point oil-gas ratio and true oil-gas ratio at the release point of the experiment may vary, as does the size distribution of the resulting oil and gas for varying released oil-gas ratios. Despite these uncertainties, a generally good 1:1 fit between the set and measured oil-gas ratios over a wide range of conditions. This provides confidence that the presented method can be used to measure oil-gas ratios, and the equivalent size distributions from within a plume of mixed oil and gas.

3.3. Spectral attenuation

Fig. 12 shows an example colour image containing a copepod (expanded in the inset). This was recorded *in situ* within Frænfjorden, Norway. While the copepod shown is a relatively large zooplankton, the details of the body and internals are adequately resolved for biometrical characterisation.

Following background correction as per Eq. (2), spectral transmittances through each pixel can be calculated. The shape of the transmitted spectra can be used as a more quantifiable metric for certain types of material, which can be related to other measurable optical properties. Assuming the incident light is recorded from a perfectly orthogonal projection (via the lens telecentricity), and no scattered light is recorded, then the corrected image (C) can be converted into an image that is close to optical attenuation for each pixel. This proxy for spectral attenuation ($C_a(\lambda)$) can be calculated for each pixel (i,j) for each waveband (λ) of the imaging sensor, using Eq. (4):

$$C_a(i,j,\lambda) = -\frac{1}{r} ln\left(C(i,j,\lambda)\right) \tag{4}$$

where r is the path length and $C_a(i,j,\lambda)$ is an image of spectral attenuation through the transmitted components of the particles in the corrected image, $C(i,j,\lambda)$.

For particle-specific attenuation estimates, it may be possible to base the incident light intensity on a 'non-particle' area or super-pixel within the corrected image. This would effectively remove the attenuation component resulting from sub-pixel particles within

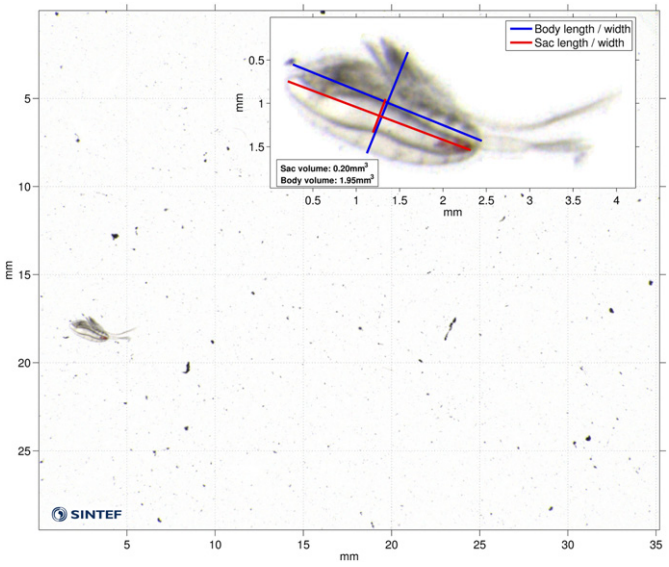

Fig. 12. Example colour image obtained within Frænfjorden, Norway. The inset shows the copepod and associated volumes of the body and lipid sack.

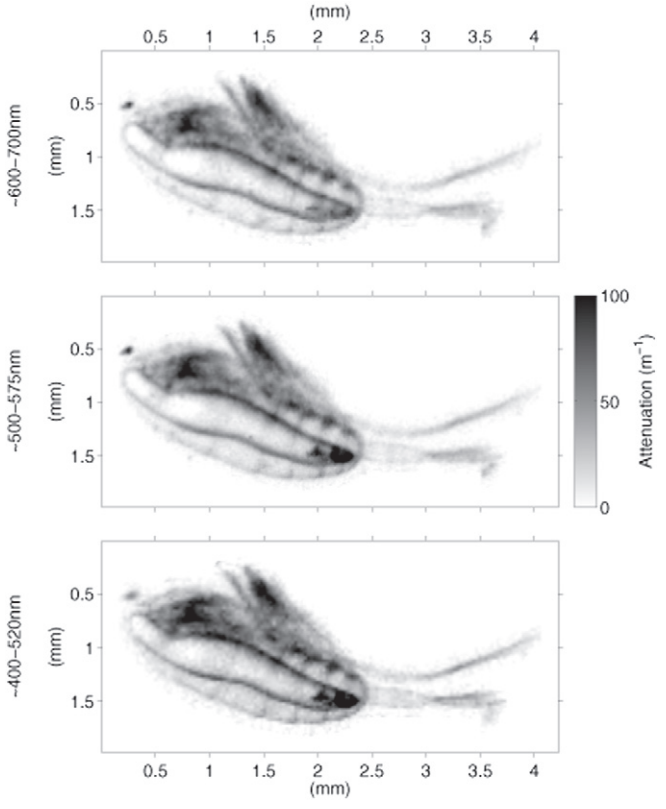

Fig. 13. Estimates of attenuation of red, green and blue light are possible to obtain for each pixel, as demonstrated in these three images of attenuation coefficients for the respective wavebands.

the water. This procedure would be required if a fixed clean-water background is used for correction. However, if an in-situ moving background is used, this will effectively have the same result of removing sub-pixel particle attenuation.

The three wavebands recorded by the system used here, enable images of attention coefficients for each of these relatively broad bands. Hyper-spectral imaging sensors could potentially be substituted into the system to enable a more detailed spectral shape to be derived (Fig. 13).

3.4. Measurements of suspended mine tailings in a Norwegian Fjord

Mine tailings are the fine waste fraction resulting from the extraction of mineral ores. In some cases, these are being discharged into the marine environment, in what is known as Submarine Tailing Placement (STP). We have taken several particle measurements using the SilCam in an active STP (Frænfjorden, Norway), in order to better understand the transport and fate of mine tailings. See Ramirez-Llodra et al. (2015) for more details of STPs in general.

Fig. 14 shows a vertical profile from Frænfjorden, taken 160 m (horizontally) from the discharge location (positioned at approximately 30 m depth). Here, the SilCam (Fig. 14A) and LISST-100 (Fig. 14B) are profiled together down through the plume of discharged tailings.

When averaged between the depths of 30–40 m, the SilCam response shows a high concentration of material of approximately 400 μm in equivalent diameter. The LISST-100, on the other hand, shows a bi-modal response in the size distribution, which peaks at approximate 180 μm and also in the largest size class. This bi-modal response is likely an artefact that stems from out-of-range particles that have the potential to be aliased into multiple smaller particles when passed through the optical inversion (Davies et al., 2012). Some volume of small (less than 50 μm) particles are also reported by the LISST, which are below the lowest resolvable limit of the SilCam system used. The higher concentration reported by the SilCam, in comparison to the LISST, can be primarily attributed to the fraction of larger particles recorded by the instrument.

Differences between the two instrument responses are evidently challenging to interpret. Are the large particles reported by the SilCam real or an artefact of the image processing, for example? Here, the power of *in situ* imagery enables a manual inspection of the types of images used in creating such size distributions, examples of which are shown in Fig. 15 for the four depths indicated in Fig. 14A. At depths 2 and 3 high concentrations of large particles are clearly evident.

4. Summary & conclusions

The *in situ* particle imaging system (SilCam) presented in this article has been developed to address the need to obtain accurate

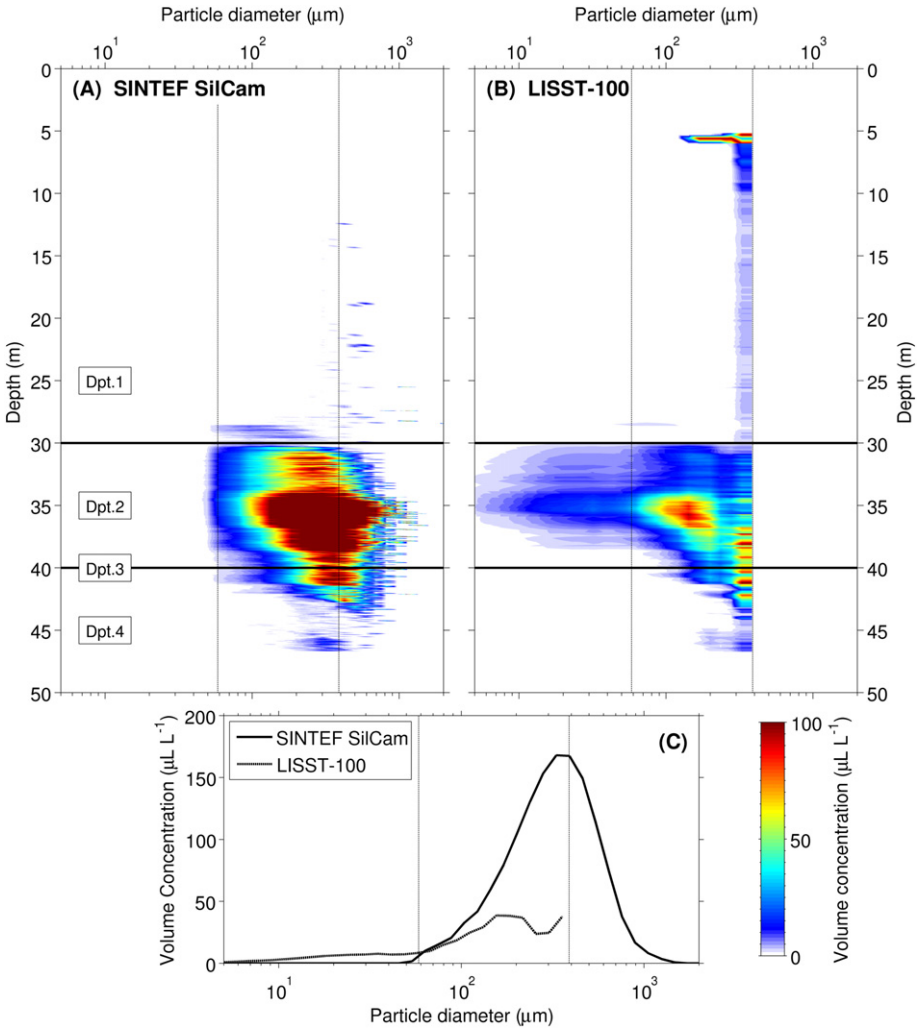

Fig. 14. Comparison of the SilCam (A) and LISST-100 (B) measurements of suspended mine tailings within Frænfjorden, Norway. The plot shown in C is for averaged size distributions from the two instruments between 30 and 40m (as indicated by the black lines in A and B.

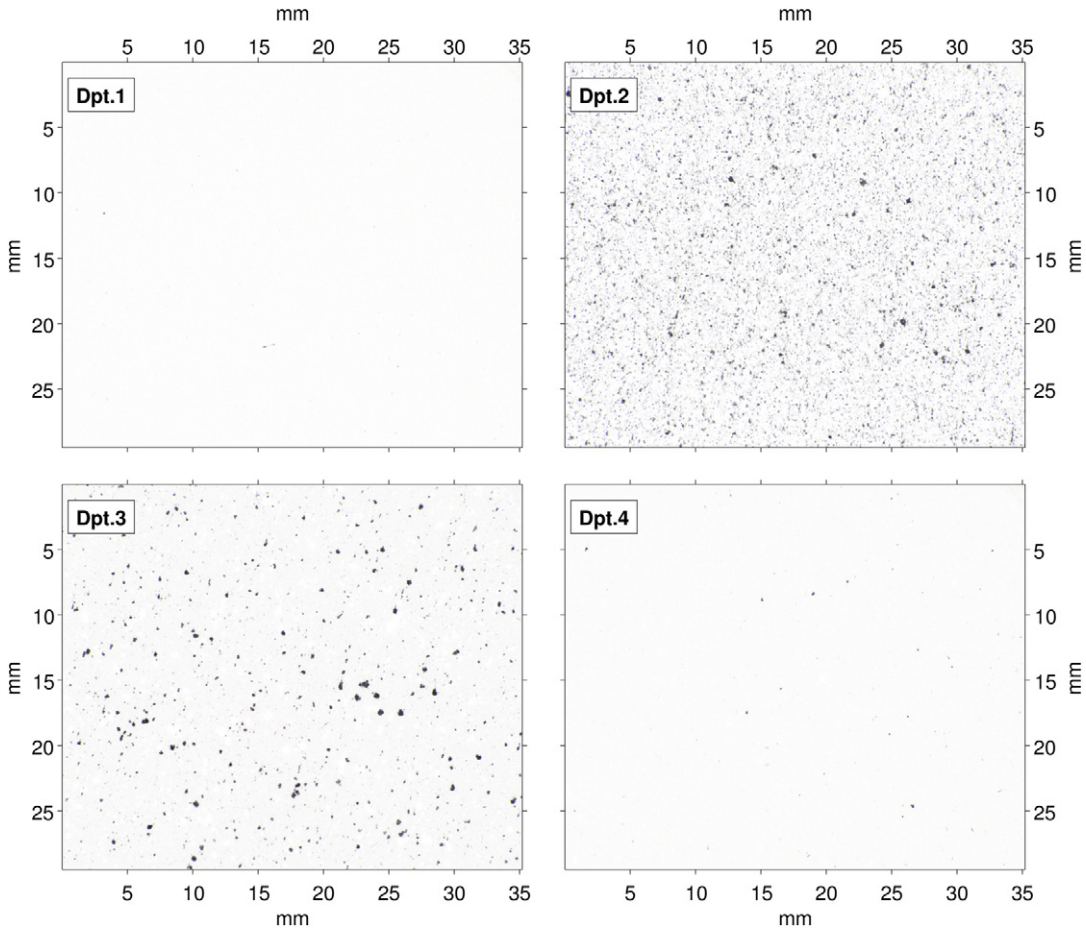

Fig. 15. Four image examples obtained with the SilCam for four depths (25, 35, 40 and 45 m), as indicated in Fig. 14.

measurements of suspended particles associated with acute marine pollution. This implies high concentrations of particles ranging from 50 μm to several millimetres. The system has been validated against measurements of spherical standards and compared well to oil droplet measurements from the LISST-100, when droplet sizes fell within the measurement range of both instruments. The SilCam system has both enabled extension of down-scaled blowout laboratory experiments to more realistic scales and also *in situ* measurements of suspended mine tailings, and zooplankton quantification.

The SilCam fills a gap in the concentration-size-shape space within *in situ* particle measurement technology, where sizes larger than the LISST-100 limit can be accurately characterised and discretized based on shape, size and spectral transmittance, in high concentration situations. The system also offers potential for some novel approaches to characterisation of basic optical properties of imaged particles.

Acknowledgments

The authors thank Alex Nimmo-Smith for his valuable assistance with constructing the high pressure underwater housings. Important development and verification tasks have been performed in projects funded by the American Petroleum Institute (API), especially regarding the high pressure version of the system. The research in this paper regarding the method for detecting oil droplets and gas bubbles was made possible by a grant from the Gulf of Mexico Research Initiative (Award number SA 15-19). The Frænfjorden data was collected in the NYKOS project (New Knowledge on Sea Deposits), which is funded bythe Norwegian Research Council and Norwegian Mining Industry (Project no. 236658).

References

Agrawal, Y.C., Pottsmith, H.C., 2000. Instruments for particle size and settling velocity observations in sediment transport. Mar. Geol. 168, 89–114.

Brandvik, P.J., Johansen, O., Leirvik, F., Farooq, U., Daling, P.S., 2013, aug. Droplet breakup in subsurface oil releases-part 1: experimental study of droplet breakup and effectiveness of dispersant injection.. Mar. Pollut. Bull. 73 (1), 26–319.

Curran, K.J., Hill, P.S., Milligan, T.G., 2003. Time variation of floc properties in a settling column. J. Sea Res. 49, 1–9.

Davies, E.J., Buscombe, D., Graham, G.W., Nimmo-Smith, W.A.M., 2015. Evaluating unsupervised methods to size and classify suspended particles using digital in-line holography. J. Atmos. Ocean. Technol. 32, 1241–1256.

Davies, E.J., Nimmo-Smith, W.A.M., Agrawal, Y.C., J., S.A., 2012. LISST-100 response to large particles. Mar. Geol. 307-310, 117–122.

Graham, G.W., Davies, E.J., Nimmo-Smith, W.A.M., Bowers, D.G., Braithwaite, K.M., 2012. Interpreting LISST-100X measurements of particles with complex shape using digital in-line holography. J. Geophys. Res. Oceans 117 (C5).

Graham, G.W., Nimmo-Smith, W.A.M., 2010. The application of holography to the analysis of size and settling velocity of suspended cohesive sediments. Limnol. Oceanogr. Methods 8, 1–15.

Johansen, O., Brandvik, P.J., Farooq, U., 2013. Droplet breakup in subsea oil releases - Part 2: predictions of droplet size distributions with and without injection of chemical dispersants. Mar. Pollut. 73, 327–335.

Mikkelsen, O.A., Hill, P.S., Milligan, T.G., Chant, R.J., 2005. In situ particle size distributions and volume concentrations from a LISST-100 laser particle sizer and a digital floc camera. Cont. Shelf Res. 25, 1959–1978.

Mikkelsen, O. a., Milligan, T.G., Hill, P.S., Moffatt, D., 2004. INSSECT - an instrumented platform for investigating floc properties close to the bottom boundary layer. Limnol. Oceanogr. Methods 2, 226–236. http://dx.doi.org/10.4319/lom.2004.2.226.

Milligan, T., 1996. In situ particle (floc) size measurements with the benthos 373 plankton silhouette camera. J. Sea Res. 36 (1-2), 93–100. http://dx.doi.org/10.1016/S1385-1101(96)90777-7.

Pham, C.K., Ramirez-Llodra, E., Alt, C.H.S., Amaro, T., Bergmann, M., Canals, M., Company, J.B., Davies, J., Duineveld, G., Galgani, F., Howell, K.L., Huvenne, V.A.I., Isidro, E., Jones, D.O.B., Lastras, G., Morato, T., Gomes-Pereira, J.N., Purser, A., Stewart, H., Tojeira, I., Tubau, X., Van Rooij, D., Tyler, P.A., 2014. Marine litter distribution and density in European seas, from the shelves to deep basins. PLoS ONE 9 (4). http://dx.doi.org/10.1371/journal.pone.0095839.

Ramirez-Llodra, E., Trannum, H.C., Evenset, A., Levin, L. a., Andersson, M., Finne, T.E., Hilario, A., Flem, B., Christensen, G., Schaanning, M., Vanreusel, A., 2015. Submarine and deep-sea mine tailing placements: a review of current practices, environmental issues, natural analogs and knowledge gaps in Norway and internationally. Mar. Pollut. Bull. 97, 13–35. http://dx.doi.org/10.1016/j.marpolbul.2015.05.062.

Superville, P.J., Prygiel, E., Mikkelsen, O., Billon, G., 2015. Dynamic behaviour of trace metals in the Deule River impacted by recurrent polluted sediment resuspensions: from diel to seasonal evolutions. Sci. Total Environ. 506-507, 585–593. http://dx.doi.org/10.1016/j.scitotenv.2014.11.044.

Thorne, P.D., Buckingham, M.J., 2004. Measurements of scattering by suspensions of irregularly shaped sand particles and comparison with a single parameter modified sphere model. J. Acoust. Soc. Am. 116 (5), 2876–2899.

Thorne, P.D., Hanes, D.M., 2002. A review of acoustic measurements of small-scale sediment processes. Cont. Shelf Res. 22, 603–632.

Turner, A., Millward, G.E., 2002. Suspended particles: their role in estuarine biogeochemical cycles. Estuar. Coast. Shelf Sci. 55 (6), 857–883. http://dx.doi.org/10.1006/ecss.2002.1033.

Wright, S.L., Thompson, R.C., Galloway, T.S., 2013. The physical impacts of microplastics on marine organisms: a review. Environ. Pollut. 178, 483–492. http://dx.doi.org/10.1016/j.envpol.2013.02.031.

Zhao, L., Boufadel, M.C., Socolofsky, S.A., Adams, E., King, T., Lee, K., 2014. Evolution of droplets in subsea oil and gas blowouts: development and validation of the numerical model VDROP-J. Mar. Pollut. Bull. 83 (1), 58–69. http://dx.doi.org/10.1016/j.marpolbul.2014.04.020.